

# AC impedance spectroscopy: a new equivalent circuit for titania thick film humidity sensors

P.M. Faia\*, C.S. Furtado, A.J. Ferreira

*ICEMS Coimbra, Department of Electrical Engineering and Computers, LTMEU/FCT, University of Coimbra,  
Polo 2, Pinhal de Marrocos, 3030-290 Coimbra, Portugal*

Received 19 July 2004; accepted 24 October 2004

Available online 7 December 2004

## Abstract

The variation of the electrical signal with humidity in ceramic sensors is originated by the chemical and physical sorptions of water molecules existing in the atmosphere. The aim of the work described in the present paper is to establish an equivalent electrical circuit for the case of two titania thick-film samples. It is shown, at least for the temperature of 23 °C, that the same type of circuit represents adequately these two samples for various relative humidities. Chemisorption and physisorption are responsible for the different charge transport mechanisms – ion hopping, ion diffusion and electrolytic conduction. Complex impedance data were obtained at the temperature of 23 °C and various relative humidities, in the frequency range 0.1 Hz–40 MHz. The best and simpler circuit representation we found, which gives the best fitting for the Cole–Cole and Bode plots, consists of two RC parallel circuits in series with two constant-phase elements (CPEs). The values of the electrical components are tabled and, as an example, the Cole–Cole and Bode plots fitting obtained for one of our samples, the sample B, for 87.5% RH, in the frequency range 0.1 Hz–40 MHz is shown.

© 2004 Elsevier B.V. All rights reserved.

**Keywords:** Humidity sensor; Titania; Thick film; Impedance spectroscopy; Circuit modelling

## 1. Introduction

The physical phenomena of electrical conduction and polarization which occur in a ceramic humidity sensor are usually represented by resistances and capacitances [1–4]. Some papers [5–7], however, go further on taking into consideration a Warburg impedance to explain mainly, and in more or less length, the spur presented in the Cole–Cole plots ( $-X = -X(R)$ , in  $Z = R + jX$ , i.e., minus the imaginary part versus the real one of the total impedance of the sensor). The variations observed in humidity measurements in ceramic sensors are originated by the chemical and physical adsorptions of water molecules existing in the atmosphere [8–11]. Some authors [12–14] reported that low and high humidity sensitivities are governed by different transport mechanisms, in which electronic conduction is included. It must be said

that in our samples we did not find any trace of electronic conduction, and, more, in our interpretation of the results it seems that the same mechanisms exist at both low and high humidities. However, these mechanisms participate in different proportions, which allow to separate between low and high relative humidity (RH) ranges, the limits of which are situated between 30 and 40% RH.

The electrical response of a porous material will be related to the surface moisture affinity, and the porous film microstructure, namely the dimensions and interconnections of the capillary micropores.

The rather involved behaviour of our samples is understood by measuring their complex impedances subjected to an external sinusoidal varying electric field. Conduction mechanisms are dependent on free charge carriers, while the dielectric behaviour has to do with polarization processes. Since the first work by Bauerle [15], complex impedance spectroscopy has been largely used to separate the several parts of the electrical response of ceramics, namely sensors.

\* Corresponding author. Tel.: +351 239796200; fax: +351 239796247.  
E-mail address: [faia@deec.uc.pt](mailto:faia@deec.uc.pt) (P.M. Faia).

The aim of the work described in the present paper is to establish an equivalent electrical circuit, within a frequency range, the response of which gives a good fitting for the obtained experimental data with an adequate physical comprehension based on the several known mechanisms already established and described in the literature. The best fitting was reached by heuristic reasoning after several previous attempts of various kinds of circuits, always supported by the underlying chemical and physical mechanisms. The same type of equivalent circuit represents adequately the complex impedance measurements we have obtained at the temperature of 23 °C for various relative humidities (RH) equal to 12, 17.5, 24.7, 54.7, 73.5, and 100% and at different frequencies, in the range 100 Hz–40 MHz for the sample A, and, for RH equal to 78, 87.5, and 100%, in the range 0.1 Hz–40 MHz for the sample B.

## 2. Samples and measurements

An explanation of the characteristics and fabrication of the samples as well as the description of the details related to the way measurements performed have already been described [16]. However, for the sake of an easy and satisfying understanding of the topic of this paper some essential information is given here.

Two different thick-film sensors, sensor A and sensor B, have been fabricated onto clean polished alumina wafers with a diameter of 20 mm and thicknesses of 3 mm. Over two silver paste electrodes with an interdigital pattern, an emulsion in acetone with ethyl cellulose as a temporary binder of as-received TiO<sub>2</sub> powder (purity > 99%) was spin-coated onto the substrates at low speed (250 rpm) for 30 s. The coating procedure was repeated three times for sample A, and twice for sample B, with intermediate drying and the burning off the organic binder of the previous layers at 150 °C for 15 s. Afterwards, the deposited film was heated up in air up to 800 °C at a constant rate of 10 °C/min, and maintained at that temperature for 2 h. The X-ray diffraction (XRD) showed that the TiO<sub>2</sub> phase of the films is anatase. A constant relative humidity (RH) was obtained by mixing water-saturated air (synthetic air saturated with water vapour) with dry synthetic air in a given ratio. Impedance spectra were recorded in the range 0.1–200 Hz by means of a frequency response analyzer, Solartron (model 1250), and in the range 100 Hz–40 MHz by using an impedance/gain-phase analyzer, Hewlett-Packard (model HP4194A), both with a peak voltage of 0.5 V.

## 3. Results and discussion

This section will be organized into three parts:

(a) the basic models assumed for the electrical conduction and polarization;

(b) presentation of the registered Cole–Cole and Bode plots, and their interpretation;

(c) presentation of the type of circuit adopted.

### 3.1. Basic models assumed for the electrical conduction and polarization

The electrical conduction and polarization are explained by the adsorbed water on the metal oxide surface and also on the capillary water condensation within the pores [17,18]. The porous structure of the TiO<sub>2</sub> samples favours both these processes.

Two types of adsorption of water vapour molecules take place: in the beginning chemisorption occurs then followed by physisorption. When adsorption starts on the clean oxide surface, a layer of hydroxyl groups is formed. The water vapour molecules are chemisorbed through a dissociative mechanism by which two surface hydroxyls per water molecule are formed: the hydroxyl group adsorbing on a surface Ti<sup>4+</sup> ion and the proton forming a second hydroxyl with an adjacent surface O<sup>2-</sup> ion.

It has been estimated that only one hydroxyl group is formed on each surface metal ion [10,11]. Thus the initial chemisorbed layer is tightly attached to the titania grains surface. Once this initial layer formed, it is no further affected by exposure to humidity. In the case of anatase, which is the phase of our titania sensors, it has been estimated that the desorption of the chemisorbed layer takes place around 200 °C [19].

As relative humidity (RH) increases, an additional layer of water molecules starts to be formed, on the chemisorbed one, being complete by 20% RH. Many more physisorbed layers will be joined as humidity gets higher [20]. These physisorbed layers are easily and reversibly removed by decreasing the humidity.

With more than one layer of physisorbed water molecules, water starts to be condensed into the capillary pores. The neck of the pore is filled or unfilled according to its radius and thickness of the physisorbed layer, i.e., depending on the magnitude of the relative humidity. With increasing RH, the thickness of the physisorbed layer of water gets bigger which leads to the filling of successively higher diameter necks, following the prediction of Kelvin equation:

$$r_k = \frac{2\gamma M}{\rho RT \ln \frac{P_s}{P}} \quad (1)$$

$r_k$  being the neck radius,  $\gamma$  the surface tension,  $M$  the molecular weight of water,  $\rho$  the density of water,  $R$  the gas constant,  $T$  the absolute temperature,  $P_s$  and  $P$  the water vapour pressure at saturation and the actual value, respectively. At room temperature (23 °C) and according to the above equation, water vapour starts to condense in mesopores of size 20 Å around 15% RH and continues on up to around 1000 Å under saturated atmosphere [21].

Three regimes of electrical conduction could be assumed [8,22]: (a) with only a small coverage of water, ( $\theta \ll 1$ ), on the chemisorbed hydroxyl groups, proton ( $H^+$ ) hopping dominates; (b) with a fractional coverage ( $\theta < 1$ ) of water, less than one physisorbed monolayer, hydronium ( $H_3O^+$ ) diffusion on hydroxyl groups dominates; (c) when water is abundant, with a coverage greater than one ( $\theta > 1$ ), then proton ( $H^+$ ) transfer process is dominant.

In the regime (a), adsorbed vapour molecules originate hydroxyl groups. The hydroxyl groups dissociate originating protons,  $OH^- \rightarrow O^{2-} + H^+$ , which requires a high activation energy. Protons will hop between the hydroxyl groups.

In the regime (b), each water molecule is slightly bonded with one hydroxyl group and  $H_3O^+$  will be the dominant charge carrier. Protonic migration proceeds following a chain of exchange reactions,  $H_3O^+ + H_2O \leftrightarrow H_2O + H_3O^+$  [9]. Simultaneously,  $H^+$  transfer also takes place between adjacent  $H_2O$  molecules in clusters.

In the regime (c), when the fractional water surface coverage is greater than one ( $\theta > 1$ ), then the transport mechanism is assured by  $H^+$  transfer between adjacent  $H_2O$  molecules within a continuous film. The Grotthuss chain reaction takes place [8], with  $H_3O^+$  being hydrated,  $H_3O^+ \rightarrow H_2O + H^+$ , which represents the transport mechanism energetically favoured in liquid water.

Finally, at high humidity, liquid water condenses in the pores, according to Kelvin's law, and electrolytic conduction occurs simultaneously with protonic transport [3,18].

The sensor capacitance, due to electric polarization, is also related to some sort of movement of charges in the applied alternating electric field. However, unlike the case of conduction, a translation movement is either blocked or hindered [23]. Electric polarization is related to an oscillation or reorientation of charges caused by the variation of the applied field. For the chemisorbed water molecules, as they are bound to the surface by two hydrogen bonds, they are not so free to reorient, following the external electric field, as those which are physisorbed, only singly bonded. Then the polarization, and consequently, the capacitance of the sensor will increase as less tightened are the water molecules with their neighbours, which happens as RH increases [24,25].

Adding up to molecules orientation, there is also the contribution to the polarization due to mobile charges accumulated at transitional structural places, as the two-layer model suggests [11,26]. In conclusion, it can be said that polarization is originated both by the orientation of adsorbed water molecules and mobile charges accumulated at the electrodes and pore necks.

### 3.2. Recorded Cole–Cole and Bode plots

Cole–Cole and Bode spectra of the complex impedance,  $Z(f) = R(f) + jX(f)$ , of the  $TiO_2$  thick films were recorded at different temperatures, with the relative humidity varying

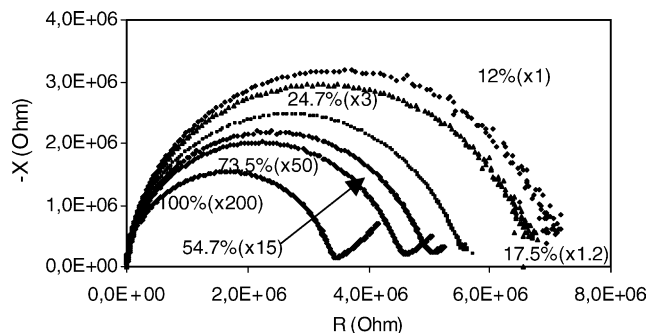


Fig. 1. Sample A – The measured Cole–Cole plots, in the 100 Hz–40 MHz range, at the temperature of 23 °C, for different RHs.

from 12 to 100% [16]. As it is well known,  $R$  is the resistance,  $X$  the reactance of the sample and  $f$  the frequency of the applied voltage. In this paper, only the results obtained at the temperature of 23 °C are reported, just because that is sufficient to give support to what we are interested: the proposal of a type of an equivalent electrical circuit for the sensor. As far as the frequency range is concerned, sample A has been measured in the 100 Hz–40 MHz range, while for sample B the range used was 0.1 Hz–40 MHz. In order to be included in the same plane, the diagrams are multiplied by appropriate factors (in brackets).

The Cole–Cole plots, shown in Figs. 1 and 2, give a more direct and easy understanding of the conduction processes involved. It can be noticed that their areas shrink with increasing RH. At a sufficiently high RH, the Cole–Cole plots are composed by elongated semicircles prolonged by curved lines for the low values of frequency. This behaviour is basically explained by two relaxation mechanisms, with not very different time constants, for the higher frequencies and by diffusion charge transport, more dominant at lower frequencies.

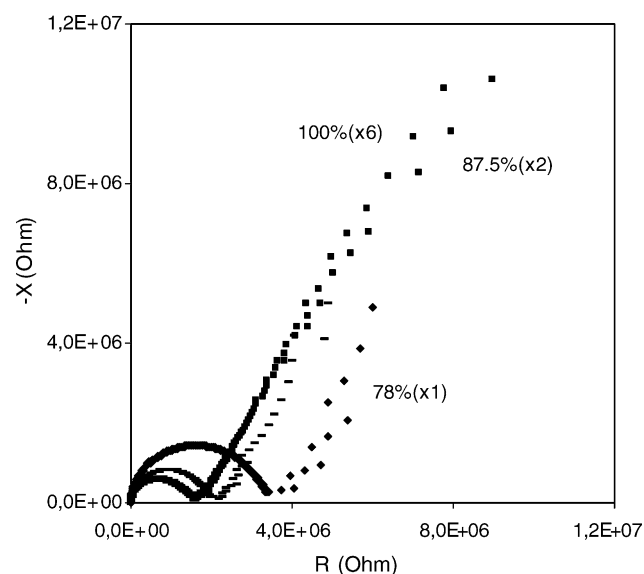


Fig. 2. Sample B – The measured Cole–Cole plots, in the 0.1 Hz–40 MHz range, at the temperature of 23 °C, for different RHs.

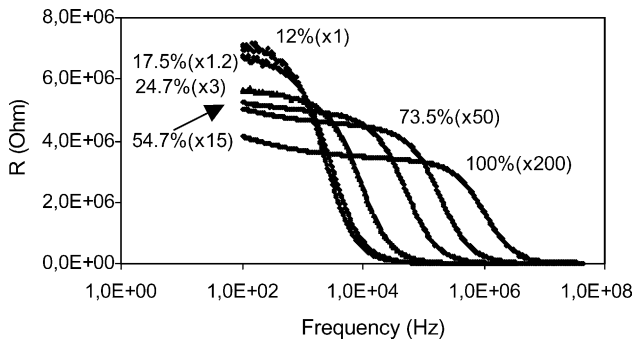


Fig. 3. Sample A – The measured Bode plots,  $R=R(f)$ , in the 100 Hz–40 MHz range, at the temperature of 23 °C, for different RHs.

The Bode plots (Figs. 3–6) confirm the suggestions given by the Cole–Cole plots. At the higher frequencies, the observed shapes are typical of relaxation mechanisms expressed by the RC parallel circuits. At the lower frequencies, typical diffusion mechanisms traduced by constant-phase elements (CPEs) are evidenced.

These considerations were taken as an orientation for the choice of the type of equivalent electrical circuit of the sensor, as it is described below.

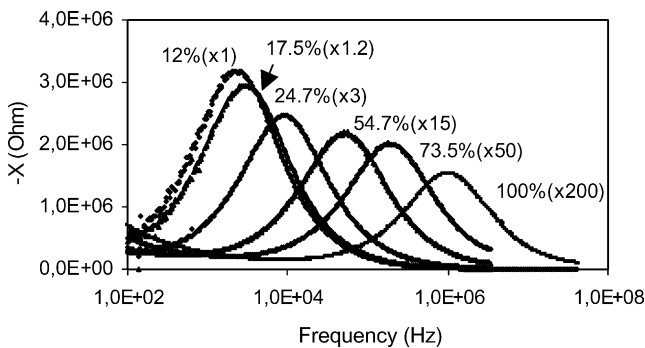


Fig. 4. Sample A – The measured Bode plots,  $-X=-X(f)$ , in the 100 Hz–40 MHz range, at the temperature of 23 °C, for different RHs.

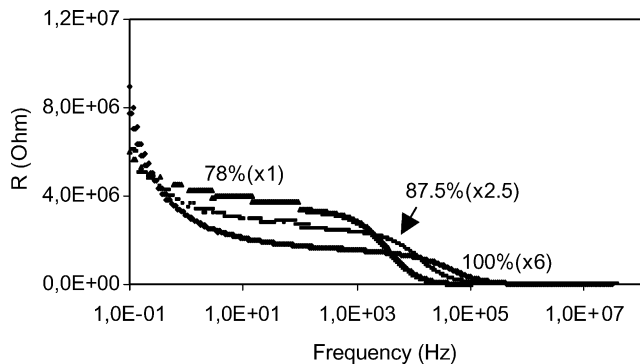


Fig. 5. Sample B – The measured Bode plots,  $R=R(f)$ , in the 0.1 Hz–40 MHz range, at the temperature of 23 °C, for different RHs.

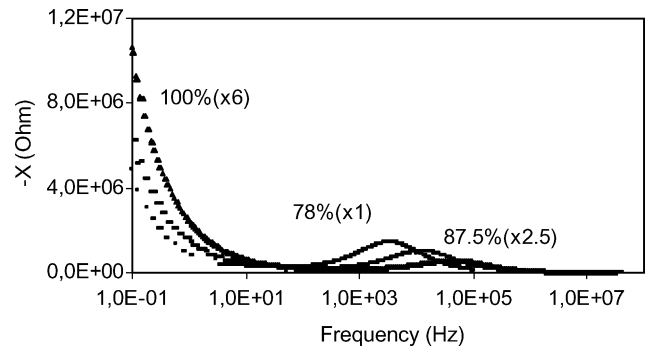


Fig. 6. Sample B – The measured Bode plots,  $-X=-X(f)$ , in the 0.1 Hz–40 MHz range, at the temperature of 23 °C, for different RHs.

As it is well known, the RC parallel circuit impedance is given by

$$Z_{R||C} = \frac{R}{1 + \omega^2 C^2 R^2} - j \frac{\omega CR}{1 + \omega^2 C^2 R^2} \quad (2)$$

with the angular frequency  $\omega = 2\pi f$ .

The corresponding Cole–Cole plot,  $-X=-X(R)$ , is a semicircle, whose diameter is equal to  $R$ , and the angular frequency  $\omega_p$  at which the peak occurs obeys to the equation

$$\omega_p RC = 1 \quad (3)$$

The constant-phase element (CPE) has a complex impedance given by [27]

$$Z_{CPE} = Af^{-n} \left( \cos \left( \frac{n\pi}{2} \right) - j \sin \left( \frac{n\pi}{2} \right) \right) \quad (4)$$

represented in the Cole–Cole plot by a straight line making an angle of  $n\pi/2$  with the abscissae ( $R$ ) axis. It must be said that the CPE-like response is always well approximated only over a finite range of frequency [28].

We think that CPEs represent what occurs at the electrodes–water layer and at the water molecules layers interface as well as inside the filled pores.

### 3.3. The type of circuit adopted

AC equivalent circuits for thick-film humidity sensors, which represent the effect of moisture on the electrical conduction and polarization of the material have been proposed by several authors [1,4,22,29–32].

In general, for a given data set there exists more than one equivalent circuit which gives a reasonable fitting. The choice between these ones has to be based both in simplicity and consistency with the known physical and chemical processes which take place in the system [33,34]. The best fittings were reached after several attempts. All the complex impedance plots obtained, Cole–Cole and Bode ones, were modelled, obeying the above criteria, by the equivalent circuit shown in Fig. 7.

$C_{geo}$  is the geometrical capacitance. It has been measured without any film, only with the electrodes deposited on the wafer.

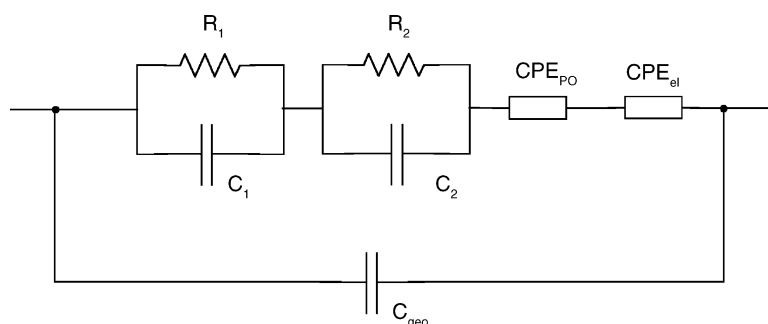


Fig. 7. The equivalent circuit of samples A and B, for different RHs.

Table 1  
Values of the equivalent electrical circuit parameters of sample A, for different RHs

RH (%)	$R_1 \parallel C_1$		$R_2 \parallel C_2$		CPE <sub>el</sub>		CPE <sub>po</sub>		$C_{geo}$
	$R_1$	$C_1$	$R_2$	$C_2$	$A_{el}$	$n_{el}$	$A_{po}$	$n_{po}$	
12	4.50E+6	8.00E–12	1.85E+6	5.20E–11	1.85E+6	0.20	–	–	3.00E–12
17.5	3.40E+6	8.80E–12	1.50E+6	5.00E–11	1.80E+6	0.21	–	–	3.00E–12
24.7	1.11E+6	8.20E–12	5.85E+5	4.00E–11	6.00E+5	0.25	–	–	3.00E–12
54.7	2.00E+5	7.80E–12	1.02E+5	3.90E–11	1.45E+5	0.24	1.00E+5	0.8	3.00E–12
73.5	5.80E+4	7.00E–12	2.60E+4	5.00E–11	4.20E+4	0.22	1.60E+5	0.7	3.00E–12
100	1.16E+4	8.40E–12	4.00E+3	6.20E–11	9.90E+3	0.20	4.70E+4	0.62	3.00E–12

The parallel  $R_1$ ,  $C_1$  represents the hopping of hydronium ions,  $H_3O^+$ , and the parallel  $R_2$ ,  $C_2$  the hopping of protons  $H^+$ . We believe that the charge carriers are correctly assigned, because: (a)  $R_1$  is in all cases greater than  $R_2$ , since the activation energy of conduction for  $H_3O^+$  is greater than that of  $H^+$ ; (b)  $C_2$  is greater than  $C_1$  because  $H^+$  ions follow more easily the variations of the alternating field than the  $H_3O^+$  ions.

Diffusion causes a CPE behaviour [35], which is reinforced by inhomogeneities in the dimensions and shape of the capillary pores. Surface roughness has also been considered as an important contributing factor [36].

In the filled pores, the mechanism is under diffusion control, as it is assumed that the kinetics of the charge transfer at the water surface layer-filled pores interfaces is much faster than the diffusion of  $H_3O^+$  ions inside the pores [35]. In such a case, the diffusional contribution to the impedance is of the CPE-type.

The interfacial character of the impedance makes it partly capacitive as well resistive in nature.

CPE<sub>el</sub> is related to the electrodes–water layer interface with values of  $n_{el}$  around 0.2–0.25, and those of  $A_{el}$  decreasing with the decrease of RH. CPE<sub>po</sub> has to do with the contri-

bution of the pores: the values of  $n_{po}$  and  $A_{po}$  decrease with the RH increase.

From Table 1, it can be seen that for the sample A, a good fitting for the lower values of RH (12, 17.5, and 24.7%) can be obtained considering only CPE<sub>el</sub>. This means that we always have the influence of the electrodes–water layer interface diffusion, while the influence of the capillary mesopores is only operative for the higher values of RH, when water is condensed inside the mesopores, what in our measurements occurs above the value of 54.7% RH.

Tables 1 and 2 show the best values obtained for the circuit elements of samples A and B, respectively.

As an example, we show the Cole–Cole plots fittings obtained for the sample B (Figs. 8–11), at 23 °C and at 87.5% RH: (a) in the range 0.1 Hz–40 MHz and (b) in the range 100 Hz–40 MHz, to get a more visible discrimination of the good fitting obtained at the higher frequencies, between 100 Hz and 40 MHz; and (c) the Bode plots in the 0.1 Hz–40 MHz range.

As a further confirmation of the attribution of CPE<sub>po</sub> to the charge transport related to the pores, we show in Table 3 for different RHs the maximum frequency, obtained by sim-

Table 2  
Values of the equivalent electrical circuit parameters of sample B, for different RHs

RH (%)	$R_1 \parallel C_1$		$R_2 \parallel C_2$		CPE <sub>el</sub>		CPE <sub>po</sub>		$C_{geo}$
	$R_1$	$C_1$	$R_2$	$C_2$	$A_{el}$	$n_{el}$	$A_{po}$	$n_{po}$	
78	1.70E+6	1.50E–11	1.20E+6	6.20E–11	9.10E+5	0.16	9.60E+5	0.69	3.00E–12
87.5	4.90E+5	1.70E–11	3.90E+5	6.10E–11	3.20E+5	0.17	5.20E+5	0.69	3.00E–12
100	1.20E+5	1.60E–11	1.00E+5	7.00E–11	1.15E+5	0.14	4.10E+5	0.67	3.00E–12

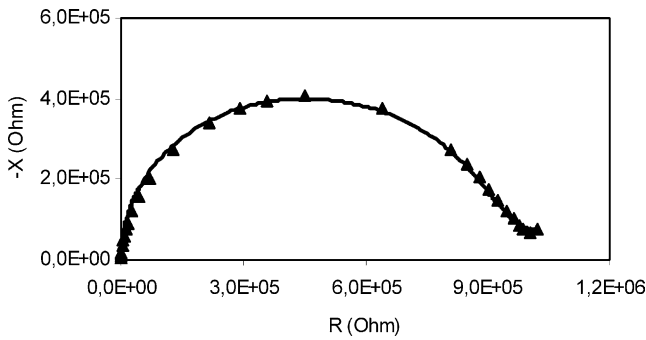


Fig. 8. Sample B – Cole–Cole plots at 87.5% RH and 23 °C, for the frequency range 100 Hz–40 MHz: (▲) experimental points; (—) simulated response of the equivalent circuit.

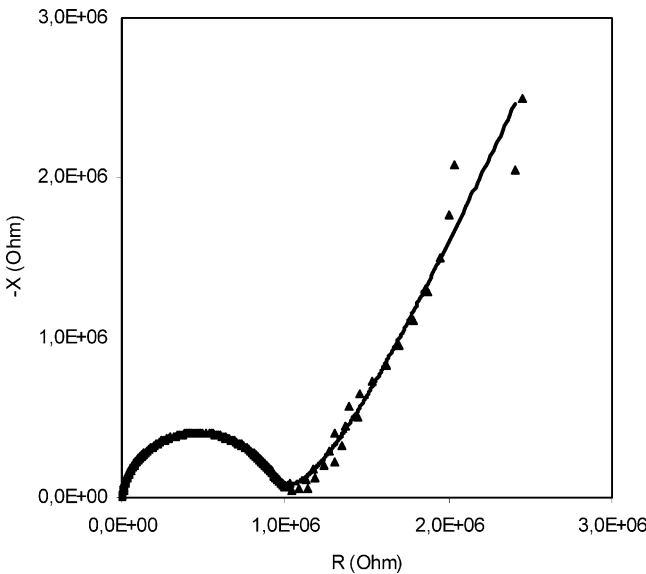


Fig. 9. Sample B – Cole–Cole plots at 87.5% RH and 23 °C, for the frequency range 0.1 Hz–40 MHz: (▲) experimental points; (—) simulated response of the equivalent circuit.

ulation, at which the influence of the RH condensed water inside the mesopores is detected.

Our interpretation of these results lies on the fact that for higher RH, the Kelvin radius decreases which also decreases

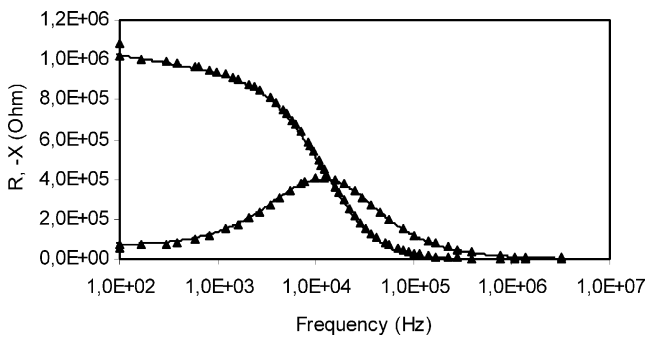


Fig. 10. Sample B — Bode plots at 87.5% RH and 23 °C, for the frequency range 100 Hz–40 MHz: (▲) experimental points; (—) simulated response of the equivalent circuit.

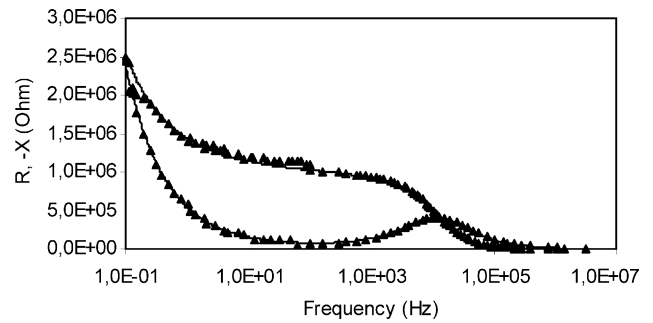


Fig. 11. Sample B – Bode plots at 87.5% RH and 23 °C, for the frequency range 0.1 Hz–40 MHz: (▲) experimental points; (—) simulated response of the equivalent circuit.

Table 3  
Maximum frequency for different RHs at which the influence of the mesopores is detected

RH (%)	Maximum frequency
≤24.7	<100 Hz
54.7	18.6 kHz
73.5	834 kHz
100	2.5 MHz

the diffusion time, and, consequently, implies the response at higher frequencies.

#### 4. Conclusion

Complex impedance data of two samples of titania thick films were recorded, at various relative humidities (RHs) and at the temperature of 23 °C, in the frequency range 0.1 Hz–40 MHz. A unique type of an equivalent electrical circuit was found to represent all the measurements performed. It is very simple, confirms the charge transport mechanisms related in the literature and is completely explained by the chemical and physical processes related to the water adsorption on the surface of metal oxide ceramics. The equivalent circuit comprehends two RC parallel circuits which represent two different relaxation processes in series with two constant-phase elements (CPEs) typical of ion diffusion and electrolytic conduction within the water condensed inside the mesopores. Cole–Cole and Bode plots are presented and interpreted on the basis of: (a) the chemisorbed and physisorbed layers of water molecules, varying with the relative humidity (RH) of the surrounding atmosphere and (b) the various transport mechanisms – ion hopping, ion diffusion and electrolytic conduction – the contribution of which is a function of the number of water layers adsorbed. Investigations to examine whether the same type of circuit is adequate to explain the dependence of complex impedance data on relative humidity (RH) in sensors with different chemical composition are going on.

## References

- [1] S. Agarwal, G.L. Sharma, Humidity sensing properties of (Ba,Sr)TiO<sub>3</sub> thin films grown by hydrothermal–electrochemical method, *Sens. Actuators B* 85 (2002) 205–211.
- [2] G. Sberveglieri, R. Murri, N. Pinto, Characterisation of porous Al<sub>2</sub>O<sub>3</sub>–SiO<sub>2</sub>/Si sensor for low and medium humidity ranges, *Sens. Actuators B* 23 (1995) 177–180.
- [3] J. Holc, J. Slunečko, M. Hrovat, Temperature characteristics of electrical properties of (Ba,Sr)TiO<sub>3</sub> thick film humidity sensors, *Sens. Actuators B* 26–27 (1995) 99–102.
- [4] M.E.V. Costa, P.Q. Mantas, J.L. Baptista, Effect of electrode alterations on the a.c. behaviour of LiO<sub>2</sub>–ZnO humidity sensors, *Sens. Actuators B* 26–27 (1995) 312–314.
- [5] Y. Li, M.J. Yang, She, Humidity sensors using “in situ” synthesized sodium polystyrenesulfonate/ZnO nanocomposites, *Talanta* 62 (2004) 707–712.
- [6] J. Wang, B. Kun Xu, S. Ping Ruan, S. Ping Wang, Preparation and electrical properties of humidity sensing films of BaTiO<sub>3</sub>/polystyrene sulfonic sodium, *Mater. Chem. Phys.* 78 (2003) 746–750.
- [7] G. Gusmano, A. Bianco, G. Montesperelli, E. Traversa, An EIS study of the humidity-sensitive electrical conduction of alkali-doped TiO<sub>2</sub> films, *Electrochim. Acta* 41 (1996) 1359–1368.
- [8] J.H. Anderson, G.A. Parks, The electrical conductivity of silica gel in the presence of adsorbed water, *J. Phys. Chem.* 72 (1968) 3362–3368.
- [9] J.J. Fripiat, A. Jelli, G. Poncelet, J. Andre, Thermodynamic properties of adsorbed water molecules and electrical conduction in montmorillonites and silicas, *J. Phys. Chem.* 69 (1965) 2185–2197.
- [10] E. McCafferty, A.C. Zettlemoyer, Adsorption of water vapour on α-Fe<sub>2</sub>O<sub>3</sub>, *Discuss. Faraday Soc.* 52 (1971) 239–263.
- [11] T. Morimoto, M. Nagao, F. Tokuda, The relation between the amounts of chemisorbed and physisorbed water on metal oxides, *J. Phys. Chem.* 73 (1969) 243–248.
- [12] R.K. Nahar, V.K. Khanna, Ionic doping and inversion of the characteristic of thin film porous Al<sub>2</sub>O<sub>3</sub> humidity sensor, *Sens. Actuators B* 46 (1998) 35–41.
- [13] V.K. Khanna, R.K. Nahar, Carrier transfer mechanisms and Al<sub>2</sub>O<sub>3</sub> sensors for low and high humidities, *J. Phys. D: Appl. Phys.* 19 (1986) 141–146.
- [14] R.K. Nahar, V.K. Khanna, W.S. Khokle, On the origin of the humidity sensitive electrical properties of porous alumina oxide, *J. Phys. D: Appl. Phys.* 17 (1984) 2087–2095.
- [15] J.E. Bauerle, Study of solid electrolyte polarization by a complex admittance method, *J. Phys. Chem. Solids* 30 (1969) 2657–2670.
- [16] P.M. Faia, C.S. Furtado, A.R. Ferreira, Humidity sensing properties of a thick-film titania prepared by a slow spinning process, *Sens. Actuators B: Chem.* 101 (2004) 183–190.
- [17] B.M. Kulwicki, Ceramic sensors and transducers, *J. Phys. Chem. Solids* 45 (1984) 1015–1031.
- [18] B.M. Kulwicki, Humidity sensors, *J. Am. Ceram. Soc.* 74 (1991) 697–708.
- [19] M. Egashira, M. Nakashimo, S. Kawasumi, Temperature programmed desorption study of water adsorbed on metal oxides. 2. Tin oxide surfaces, *J. Phys. Chem.* 85 (1981) 4125–4130.
- [20] W.M. Sears, The effect of oxygen stoichiometry on the humidity sensing characteristics of bismuth iron molybdate, *Sens. Actuators B* 67 (2000) 161–172.
- [21] K.-S. Chou, T.-K. Lee, F.-J. Liu, Sensing mechanism of a porous ceramic as humidity sensor, *Sens. Actuators B* 56 (1999) 106–111.
- [22] Y.-C. Yeh, T.-Y. Tseng, D.-A. Chang, Electrical properties of TiO<sub>2</sub>–K<sub>2</sub>Ti<sub>6</sub>O<sub>13</sub> porous ceramic humidity sensor, *J. Am. Ceram. Soc.* 73 (1990) 1992–1998.
- [23] W.J. McCarter, Effects of temperature on conduction and polarization in Portland cement mortar, *J. Am. Ceram. Soc.* 78 (1995) 411–415.
- [24] M.G. Baldwin, J.C. Morrow, Dielectric behavior of water adsorbed on alumina, *J. Chem. Phys.* 36 (1962) 1591–1593.
- [25] K.S. Cole, R.H. Cole, Dispersion and absorption in dielectrics. I. Alternating current characteristics, *J. Chem. Phys.* 9 (1941) 341–351.
- [26] T. Morimoto, T. Iwaki, Dielectric behaviour of adsorbed water – Part 1, *J. Chem. Soc., Faraday Trans. 1* 83 (1987) 943–956.
- [27] J.R. MacDonald, C.A. Hull, Pseudo-reaction rate in the AC response of an electrolytic cell, *J. Electroanal. Chem.* 165 (1984) 9–20.
- [28] J.R. MacDonald, G.B. Cook, Analysis of impedance data for single crystal Na beta-alumina at low temperatures, *J. Electroanal. Chem.* 168 (1984) 335–354.
- [29] P.M. Faia, C.S. Furtado, A.R. Ferreira, J.M. Peidigão, Humidity and methane sensitivity measurements on a TiO<sub>2</sub> thick-film materials 2003, Caparica, Portugal, April 14–16, 2003.
- [30] G. Gusmano, G. Montesperelli, P. Nunziante, E. Traversa, Study of the conduction mechanism of MgAl<sub>2</sub>O<sub>4</sub> at different environmental humidities, *Electrochim. Acta* 38 (1993) 2617–2621.
- [31] N. Hirose, A.R. West, Impedance spectroscopy of undoped BaTiO<sub>3</sub> ceramics, *J. Am. Ceram. Soc.* 79 (1996) 1633–1641.
- [32] J.R. MacDonald, *Impedance Spectroscopy*, Wiley, New York, 1987, p. 97.
- [33] J.R. MacDonald, *Impedance Spectroscopy*, Wiley, New York, 1987, p. 23.
- [34] J.R. MacDonald, *Impedance Spectroscopy*, Wiley, New York, 1987, p. 83.
- [35] J. Wang, Q. Lin, R. Zhou, B. Xu, Humidity sensors based on composite material of nano-BaTiO<sub>3</sub> and polymer RMX, *Sens. Actuators B* 81 (2002) 248–253.
- [36] S.-H. Song, X. Wang, P. Xiao, Effect of microstructural features on the electrical properties of TiO<sub>2</sub>, *Mater. Sci. Eng. B* 94 (2002) 40–47.

## Biographies

**Pedro M. Faia** received his degree in Electrical Engineering (1990), is M.S. in Automation (1994) and is Ph.D. in Electronic Materials (2003) from the University of Coimbra. He is an Auxiliary Professor at the Department of Electrical Engineering and Computers of the University of Coimbra where his research interests concern the research and development of solid state chemical sensors, sensor integration techniques and software projects development for VLSI technology.

**Carlos S. Furtado** received a D. Phil. in Physics from Oxford University (1971) and an Aggregation Degree from Coimbra University (1974). He is full professor at the Department of Electrical Engineering and Computers of the University of Coimbra with interests in electronic ceramics and gas sensors.

**António J. Ferreira** graduated in Electrical Engineering (1976) and received his Ph.D. (1994) from the University of Coimbra. He is currently Associated Professor at the Department of Electrical Engineering and Computers of the University of Coimbra, with interests in various areas of electrical properties of materials, ferrites, ceramics and gas sensors, having particular interest in Impedance Spectroscopy analysis technique.